Network analysis links genome-wide phenotypic and transcriptional stress responses in a bacterial pathogen with a large pan-genome.

Paul A. Jensen,[1,2†] Zeyu Zhu,[1†] and Tim van Opijnen[1*]

1. Biology Department, Boston College, Chestnut Hill, MA, USA
2. Current address: Department of Bioengineering and Carl R. Woese Institute for Genomic Biology, University of Illinois at Urbana-Champaign, Urbana, IL, USA

† Equal contribution

* Corresponding author

E-mail Addresses:

PAJ: pjens@illinois.edu

ZZ: zhuzd@bc.edu

TvO: vanopijn@bc.edu (corresponding)

Keywords:

Tn-Seq

RNA-Seq

stress response

Streptococcus

systems biology

data integration

metabolic modeling

ABSTRACT

Background: Bacteria modulate subcellular processes to handle stressful environments. Genome-wide profiling of gene expression (RNA-Seq) and fitness (Tn-Seq) allows two views of the same genetic network underlying these responses. However, it remains unclear how they combine, enabling a bacterium to overcome a perturbation.

Results: Here we generate RNA-Seq and Tn-Seq profiles in three strains of *S. pneumoniae* in response to stress defined by different levels of nutrient depletion. These profiles show that genes that change their expression and/or become phenotypically important come from a diverse set of functional categories, and genes that are phenotypically important tend to be highly expressed. Surprisingly, we find that expression and fitness changes rarely occur on the same gene, which we confirmed by over 140 validation experiments. To rationalize these unexpected results we built the first genome-scale metabolic model of *S. pneumoniae* showing that differential expression and phenotypic importance actually correlate between nearest neighbors, although they are distinctly partitioned into small subnetworks. Moreover, a meta-analysis of 234 *S. pneumoniae* gene expression studies reveals that essential genes and phenotypically important subnetworks rarely change expression, indicating that they are shielded from transcriptional fluctuations and that a clear distinction exists between transcriptional and phenotypic response networks.

Conclusions: We present a genome-wide computational/experimental approach that contextualizes changes that occur on transcriptomic and phenomic levels in response to stress. Importantly, this highlights the need to connect disparate response networks, for instance in antibiotic target identification, where preferred targets are phenotypically important genes that would be overlooked by transcriptomic analyses alone.

INTRODUCTION

How organisms handle and overcome stress in their environment is a central question in biology, with applications in fields ranging from bioengineering to drug(-target) discovery. With the advent of genome-wide approaches, it has become clear that even relatively simple perturbations, such as a change in extracellular pH or the presence of an antibiotic, require complex physiologic responses affecting multiple subcellular processes [1-7]. A complete cellular stress response can be separated into at least two organization levels. The *transcriptional response* describes the change in gene expression following stress, while the *phenotypic response* describes how the importance of each gene (fitness) changes due to stress. Although the transcriptional and phenotypic stress responses are inter-dependent, they are measured experimentally by two disparate technologies. Transcriptomic profiling, as measured by cDNA microarrays or RNA-Seq, has been particularly popular in deciphering the complex bacteria-environment interaction to identify genes that change in their transcript abundance upon various environmental perturbations, such as exposure to antibiotics [8,9], interaction with host niches [10], and disruption of iron homeostasis [11]. Although such profiles provide a detailed picture of the transcriptional landscape, it remains to be determined whether transcript abundance alone is predictive of the phenotypic importance of a gene [12,13]. Alternatively, genome-wide mutant fitness profiling approaches, such as transposon insertion sequencing (Tn-Seq), have been developed to directly link genotypes to phenotypes and thereby measure the phenotypic stress response on a genome-wide scale [14-18]. This means that Tn-Seq determines the phenotypic importance of each gene in the genome in a specific environment (referred to as “gene fitness” in this paper) by measuring the effect each gene knockout in the genome has on fitness. For example, the lower the fitness, the more important a gene is for maintaining survival under a specific (e.g. stressful) condition [2,14,18]. Although both transcriptomic and phenotypic fitness profiling interrogate the same gene network, little is known about how these two data types correlate, i.e. are differentially expressed genes also phenotypically important during stress? Indeed, it is generally assumed that differentially expressed genes also represent phenotypically important genes. However, this assumption has not been thoroughly investigated, raising the possibility that if transcriptional and phenotypic stress responses are not correlated, then measuring either one alone offers an incomplete and incorrect picture of the cellular response. Here we determine

whether a correlation between transcription and phenotype exists and whether these stress responses can be combined to obtain a complete physiologic response.

As our model system we employ the human pathogenic bacterium *Streptococcus pneumoniae*, a major respiratory pathogen and source of morbidity and mortality. *S. pneumoniae* colonizes the nasopharynx asymptomatically, but by disseminating to other tissues it can trigger disease, including pneumonia, meningitis, sepsis, and otitis media, which results in ~1 million deaths annually among children <5 years of age and ~0.5 million among groups including the immunocompromised and the elderly (>65 years) [19-21]. One possible challenge in exploring the physiologic response in a species such as *S. pneumoniae* is the genomic variation among strains. The increasing availability of fully sequenced genomes for this and other species has demonstrated a distinction between the species' core genome (the set of genes shared by all strains) and its pan-genome (the species' global genetic repertoire) [22-25]. Because no gene or pathway functions in a vacuum, rather they are connected by complex genetic networks [26,27], the presence or absence of genes among different pneumococcal strains suggests that each strain's genomic network may be differently wired, which could potentially make phenotypes strain-dependent. Indeed, we have recently shown that strain-specific phenotypic stress responses in *S. pneumoniae,* for instance in response to antibiotics, may be common [1]. Thus, when working with a bacterium with a large pan-genome, an ideal approach should obtain a species-wide, generalizable view of how the bacterium overcomes a stressful environment.

In this study, we investigate whether differentially expressed genes are also phenotypically important during stress in *S. pneumoniae*. We generate an unbiased, high-quality, and extensively validated profile of the bacterial stress response by employing two genome-wide approaches, RNA-Seq and Tn-Seq, to measure both the transcriptional and phenotypic stress response for three pneumococcal strains under three different levels of nutrient depletion. Surprisingly, there is little correlation between differential expression and phenotypic importance across the entire genome. To contextualize the transcriptional and phenotypic profiles, we built and curated the first genome-scale metabolic model in the genus *Streptococcus*. By integrating all our data into this model we show that the disparate genes with expression and fitness changes are actually closely connected in the genomic network. However, phenotypically important and essential genes seem to be transcriptionally shielded from large

fluctuations in expression and therefore organizationally separated from transcriptionally plastic, but phenotypically unimportant, genes. Importantly, we provide a detailed roadmap to develop similar systems-level approaches in other microorganisms. Our approach facilitates profiling and reconciling transcriptomic and mutant fitness datasets and enables mapping of an organism's full physiologic response to an environmental disturbance. Moreover, this study provides a clear rationale that emphasizes the importance of targeting phenotypically important genes rather than differentially expressed genes in applications such as in drug target discovery.

RESULTS AND DISCUSSION

Designing a robust nutrient depletion assay for *S. pneumoniae*. To avoid bias in the bacterial response to nutrient depletion that might result from genomic variation in a particular strain, we selected three phylogenetically distant strains to represent *S. pneumoniae*: TIGR4 (T4), Taiwan-19F (19F) and D39 (**Additional File 1**). Both T4 and 19F can cause invasive pneumococcal disease (IPD): T4 is a serotype 4 strain that was originally isolated from a Norwegian patient with IPD [28,29]; 19F is a multi-drug resistant strain isolated from a patient with IPD in Taiwan [30,31] (**Table 1**). D39 is a historically important and commonly used serotype 2 strain that was originally isolated from a patient about 90 years ago [32] (**Table 1**). Concerning their genomic content, the three strains share 1647 genes, while T4 has 217, 19F has 140 and D39 has 93 strain-specific genes (**Additional Files 2 and 3**). To simulate systemic nutrient depletion, we designed three increasingly restrictive media to cultivate *S. pneumoniae*. The first, semi-defined minimal media (SDMM), is a relatively rich media we have used previously [1,2] that contains a single carbon source (glucose), yeast extract, casein hydrolysate (digested amino acids), salts, trace metals, and vitamins (**Table 2**). The second, a chemically defined media (CDM), is based on a previously described recipe [33], however the original composition did not allow each strain to grow robustly. By adjusting the recipe, mainly by taking SDMM as the basis and replacing the yeast extract and casein hydrolysate by an equimolar mixture of the 20 amino acids, comparable growth rates to SDMM are achieved. CDM is thus completely defined, is less nutrient rich then SDMM, but still contains several non-essential components. By iteratively removing components of CDM, we created a minimal CDM, or MCDM, that still enables each strain to grow. In contrast to SDMM and CDM, each component in MCDM is essential for growth in at least one of the three strains, and removing any component of MCDM triggers severe growth defects in at least one strain. Nutrient availability therefore decreases from SDMM to CDM, and further to MCDM (**Additional File 4)**, which is illustrated by a decrease in the growth rate of *S. pneumoniae* (**Table 1, Additional File 5**). By using multiple strains and three media conditions, generalizable -- instead of strain and/or environment-specific -- profiles are assembled that map the phenotypic and transcriptomic stress responses.

Genome-wide fitness and expression profiling reveal the phenotypic and transcriptional importance of cellular processes upon nutrient depletion. We applied two high-throughput, genome-wide methods to determine on two different levels how *S. pneumoniae* deals with nutrient depletion stress. The first level is measured by Tn-Seq, which quantifies a gene's effect on the growth rate (fitness) resulting from a genetic disruption by transposon insertions [18]. The second level is determined by RNA-Seq, which measures gene expression by quantifying transcript abundance. Tn-Seq fitness data thus provides insight into the phenotypic importance of each gene, while RNA-Seq provides insight into which genes respond to stress on a transcriptional level.

Six transposon insertion libraries for each strain were constructed and grown in each media to generate Tn-Seq profiles and a comprehensive genotype-phenotype map for each strain/environment pair (**Figure 1a**). As expected, and as we have shown before [1,2,14], the majority of insertions do not produce a significant fitness change, and more fitness defects (fitness < 1) were observed than increases in fitness (fitness > 1) (**Additional File 6**). To complement the Tn-Seq fitness data, genome-wide gene expression was measured for each strain/media pair by RNA-Seq. Four replicates from mid-exponential phase cells were prepared for each strain/media pair and sequenced at high depth (3.5-16 million reads/sample) [34]. Each sample contained reads mapping to 88-96% of all annotated genes in the corresponding genome, and transcript abundance between genes varied by nearly 10^5 (**Figure 1b, Additional File 6**). Comparing the raw expression value (i.e. transcript abundance, not fold change) with fitness revealed that most genes with a fitness defect are highly expressed (**Figure 1c**), which is a pattern that holds across all strains and all three media. However, this pattern is of little predictive value, since the majority of highly expressed genes do not have a fitness defect or increase, and thus transcript abundance alone does not predict fitness.

Validation experiments confirm that high-throughout profiles consist of high confidence data. The high-throughput genome-wide approaches Tn-Seq and RNA-Seq provide comprehensive profiles of cell physiology at two different levels. However, as with any high-throughput experiment the resulting datasets require careful validation to assess their accuracy. Tn-Seq data were validated by constructing 31 individual gene deletion mutants across the three strains. The mutants were used in monoculture growth

assays and 1x1 competition assays in which the wild type strain is competed against the mutant to obtain fitness. In total 122 genotype-phenotype relationships were validated across the three strains and three media conditions, which to our knowledge is the largest validation set generated to date for different strains of a bacterial pathogen for which no ordered knockout arrays exist. This resulted in a strong correlation (R^2 = 0.82), which is similar to correlations we achieved previously [1,2] and confirms high-confidence Tn-Seq fitness data (**Figure 2a; Additional File 7**). Importantly, these data also give detailed information on what type of stress is experienced by the bacterium. For example, Tn-Seq data shows that in rich media (SDMM) Δ*aroE (SP1376),* which catalyzes the conversion of 3-dehydroshikimate to shikimate and is associated with an upstream reaction in the *de novo* synthesis pathway of aromatic amino acids, has a growth defect (SDMM: W_{aroE} = 0.75), which we indeed validated (**Figure 2b**). However, a more severe defect in growth is measured when Δ*aroE* is grown in CDM and thus under stress by limited availability of amino acids (CDM: W_{aroE} = 0.26). Moreover, the gene becomes almost conditionally lethal in MCDM in the absence of aromatic amino acids (MCDM: W_{aroE} < 0.10). These data not only show that the Tn-Seq data consist of high confidence fitness values, but it also pinpoints environment-dependent weaknesses in the genomic network, highlighting how different genes become important in an environment-dependent manner. Moreover, it shows what type of stress is experienced in the environment; the conditional importance of *aroE* suggests an increasing lack of aromatic amino acids in CDM and MCDM.

Additionally, the RNA-Seq data were validated by qPCR by measuring the expression of nine genes in the three media conditions (**Figure 2c**). The changes in expression measured by qPCR match the RNA-Seq differential expression data across all strains and media (**Additional File 8**), confirming that the generated genome-wide expression profiles represent real changes in transcription.

Identifying genetic drivers of the nutrient stress response. The validated high-throughput data were used to identify genes responsible for the phenotypic (Tn-Seq) and transcriptomic (RNA-Seq) stress responses. By comparing fitness across environments we determined which genes changed their fitness (Δfitness, or Δ*W*) as *S. pneumoniae* transitions from rich media (SDMM) to defined (CDM) or minimal (MCDM) media (**Figure 3a**). Thus genes whose importance increases upon nutrient depletion will have

a decreased fitness (*i.e.* a negative Δfitness) in the more restrictive media, while those whose importance does not change will have a Δfitness of 0. Those genes whose importance decreases will have an increased fitness (*i.e*. a positive Δfitness). Following a change from SDMM to either CDM or MCDM, each strain had an average of 12 genes increase in fitness and 29 genes decrease in fitness. For example, gene *SP1555* (dihydrodipicolinate reductase) is a key enzyme for lysine biosynthesis. A deletion of *SP1555* thus blocks *de novo* lysine synthesis and should hamper *S. pneumoniae*'s ability to overcome the depletion of extracellular lysine in CDM and MCDM. Indeed, Tn-Seq data shows that *SP1555* is not important in rich media (SDMM: W_{SP1555} = 0.95), but shows decreasing fitness, and thus increasing importance, in the more stringent media (CDM: W_{SP1555} = 0.78, ΔW_{SP155} = - 0.17; MCDM: W_{SP155} = 0.07, ΔW_{SP155} = - 0.71).

Besides genes that change in fitness, genes that change in expression were identified by comparing transcript abundances between SDMM and either CDM or MCDM (**Figure 3b**). On average, the media shift caused 101 genes to significantly increase expression and 125 genes to decrease expression. Overall, 5.4 times more genes showed significant expression changes compared to significant fitness changes. Importantly, in both the Tn-Seq and RNA-Seq datasets, the significant changes were distributed across a variety of cellular subsystems, indicating that the nutrient depletion environments trigger stress that is experienced network-wide (**Figure 3c**). Among metabolic subsystems, amino acid pathways are especially well represented, with 17% of genes showing a fitness change and 23% of genes differentially expressed (**Additional File 6**).

Genome-wide data visualization with a whole cell model reveals that expression profiles are poor predictors of phenotypic importance. *S. pneumoniae* designates a large fraction of its genome to metabolism, and a number of metabolic enzymes have been linked to the bacterium's phenotypic stress response to nutrient and antibiotic perturbations [1,2]. Given the large number of metabolic genes with fitness or expression changes during nutrient depletion (**Figure 3c**), we focused on metabolic pathways to identify patterns in how *S. pneumoniae* handles and overcomes stress. To analyze metabolism in a systematic and comprehensive way, a genome-scale metabolic model of *S. pneumoniae* was assembled. A draft metabolic model was derived from the KBase system [35] (http://kbase.us) by collecting metabolic

reactions associated with the annotated genomes for T4, 19F, and D39. To account for non-enzymatic reactions and reactions with misannotations, a gap-filling algorithm [36] added reactions to ensure growth of the model on SDMM, CDM, and MCDM. Pathways in the model were manually curated by comparing reactions and gene associations to KEGG [37] and BioCyc [38], with a particular emphasis on amino acid and nucleotide metabolism (**Additional Files 9 and 10**). The final model, called iSP16, details the interconversion of 866 metabolites by 928 reactions, catalyzed by 463 genes (43.9% of all ORFs in T4). To our knowledge, iSP16 is the first curated, genome-scale metabolic model in the genus *Streptococcus*.

Using iSP16, we searched for patterns in the location of fitness and expression changes during nutrient stress. Initially, we expected the Tn-Seq and RNA-Seq data to align, as increasing expression of a metabolic enzyme can increase flux through an important pathway [39]. However, overlaying the datasets onto the network shows that, when transitioning from SDMM to CDM, metabolic pathways either change on a transcriptional level or their fitness (phenotypic importance) changes, but they almost never change in the same location (**Figure 4a**). Moreover, upon transitioning to MCDM, the clusters of fitness or expression changes expand but they almost never merge (**Figure 4b**). This means that, contrary to our expectations (and popular belief), overlap between fitness and expression changes are incredibly rare (**Figure 4**).

A clear example of the disconnect between fitness and expression changes is the shikimate pathway, the biosynthetic route for the aromatic amino acids (**Figure 5a**). Beginning with the glycolytic and pentose phosphate pathway intermediates phosphoenol-pyruvate (PEP) and erythrose-4-phosphate (E4P), the shikimate pathway uses seven enzymatic reactions before branching in sub-pathways specific for tryptophan (Trp), phenylalanine, and tyrosine. The branchpoint occurs immediately after gene *SP1374*, with gene *SP1816* catalyzing the first reaction of the Trp-specific branch (**Figure 5a**). Compared to SDMM, CDM contains reduced tryptophan, and MCDM contains no tryptophan (**Table 2, Additional File 4**). We expected that the removal of Trp would cause increased expression of the shikimate pathway to compensate for the absence of Trp and decreased fitness when any of the pathway's genes are interrupted. Although this pathway shows both fitness and expression changes in our data, the fitness changes are restricted to the genes above the branch into tryptophan synthesis (*SP1700* - *SP1374*), while the expression changes are below the branch point (*SP1817* - *SP1812*) (**Figure 5a**). The sole biosynthetic

route to tryptophan thus contains disjoint sets of genes with fitness and expression changes, indicating that a single pathway can be split between the phenotypic and transcriptional stress responses.

Strikingly, the lack of correlation between fitness and expression changes is not limited to metabolic genes. When plotting genome-wide expression changes against fitness changes (**Figure 5b**), no clear relationship is observed between fitness and expression changes; almost all genes appear on either the horizontal or vertical axes of **Figure 5b**, indicating either a fitness change with no expression change, or vice versa. Therefore, even though fitness and expression changes occur across the genome, their disjointedness would go unnoticed if only Tn-Seq or RNA-Seq experiments were performed, suggesting that upon exposure to stress, expression profiles are not good predictors of what is actually phenotypically important in a bacterium.

Cellular networks link changes in gene expression and fitness. In the metabolic network, fitness and expression changes rarely overlap, but they often seem to be located near one another (**Figure 4**). Thus even though expression changes are not indicative of genes that are phenotypically important, expression changes suggest that phenotypically important genes are often very close neighbors. To test this hypothesis a nearest neighbor analysis was performed in which each gene with a fitness change is paired with the closest gene in the network with an expression change (**Figure 5c**). The same procedure was repeated, starting with the genes with expression changes and searching for nearby fitness changes. Importantly, the nearest neighbor transformation restores the expected relationship between increased expression and decreased fitness. Prior to considering the nearest neighbors, 33% of the genes in **Figure 5a** appeared in the upper left quadrant (decreased fitness and increased expression) (**Figure 5d**). After pairing with nearby genes, 59% of the genes moved into this quadrant, the largest change for any quadrant of the graph.

This raises at least two questions: 1.) How close, on average, are paired neighbors; and 2.) Is there a neighbor-to-neighbor relationship between the size of the fitness change and the change in expression? For instance, are genes with the largest fitness changes neighbors with genes with the largest expression changes? To answer these questions distances between genes in the metabolic network were quantified by counting the number of reactions between enzymes (**Figure 6a**). For instance, genes associated with the

same reaction have a distance of zero, while genes associated with reactions that share a common metabolite have a distance of one. To quantify the magnitude of both the fitness and expression changes, we multiply the two changes. This product corresponds to the area of a rectangle drawn between a point in **Figure 5c** and the origin (**Figure 6b**). This "area off axes" is maximized when both the fitness and expression changes are large, and it is near zero when either the fitness or expression change is small. Finally, by plotting the fitness-expression product against the distance between the corresponding genes (**Figure 6c**), two conclusions can be drawn. First, the majority of fitness and expression changes pair at short distances, with 80% of all pairs within a distance of two, and 93% within a distance of three. Second, the size of the fitness and expression changes in each pair decreases with distance ($p < 0.005$, ANOVA). This analysis (**Figure 5**) thus shows quantitatively what is visually suggested in **Figure 4**; fitness and expression changes occur in distinct, but co-localized genes. Moreover, the largest changes in fitness are close to the largest expression changes, which means that fitness and expression changes are not only co-located, but have a magnitude that matches their neighbors'.

Further visual inspection of the metabolic network maps (**Figure 4**) suggests that genes with fitness changes and genes with expression changes are not distributed evenly throughout the network. Instead, it appears that small clusters of fitness and expression changes are present, suggesting small sub-networks that either change transcriptionally or that are conditionally important. To quantify the existence of these clusters, we compared the distribution of distances among all genes, genes with fitness changes, and genes with expression changes (**Figure 6d**). Genes with an expression change (Δexpression→Δexpression) are indeed clustered at shorter distances to other differentially expressed genes, and the same is true for genes that change in fitness (Δfitness→Δfitness) ($p < 0.005$, *t*-test of Poisson fit to distributions of distances) (**Figure 6d**). In contrast, essential genes, derived from these and previous Tn-Seq data [2,14] (**Additional File 11**) are not closely clustered (**Figure 6e**, essential→essential). Instead, essential genes are closer to genes with fitness changes than they are to either genes with expression changes or other essential genes (**Figure 6e**, essential→Δessential and essential→Δfitness, $p < 0.05$). This distribution shows that: 1.) Phenotypic stress response genes lie closer to essential genes than transcriptional stress response clusters; and 2.) Both transcriptional control and important functions are intertwined, but separated into small clusters that correspond to either the phenotypic or transcriptional stress responses. Therefore, it appears

311 that genes that become phenotypically important in a new environment are shielded from highly
312 fluctuating changes in expression, while nearby genes that are less important on a phenotypic level may
313 fluctuate to a much larger extent, suggesting these different sets of genes are part of differently organized
314 regulatory modules.
315
316 **Meta-analysis reveals partitioning of phenotypic and transcriptomic stress responses across**
317 **multiple conditions.** If these distinct sets of genes are indeed organized in different regulatory modules,
318 this would suggest that essential genes and the phenotypically important genes we identified would be
319 universally shielded from expression changes across any condition. To test this hypothesis, we performed
320 a meta-analysis using all publicly available *S. pneumoniae* datasets in the Gene Expression Omnibus
321 (GEO) database. Using microarray data from 234 experiments (**Additional File 9**), we calculated the
322 "expression plasticity" across a wide range of genetic and environmental perturbations (**Figure 7a**). The
323 plasticity is the relative variance in expression of the gene (and its homologs) across all datasets in the
324 GEO database. This means that genes with low plasticity rarely vary in their expression levels, while
325 high plasticity genes vary widely in their expression across conditions. The GEO meta-analysis shows
326 that both essential genes (which are phenotypically important in all environments) as well as genes with
327 fitness changes in our dataset have low expression plasticity across the GEO datasets (**Figure 7b**).
328 Furthermore, plotting the GEO expression plasticity against the size of the fitness change in our
329 experiment reveals that genes with the largest fitness changes have the lowest plasticity (**Figure 7c**).
330 And thus, not only do the phenotypically important genes have no corresponding expression change in
331 our experiments, they also hold their expression relatively constant across all the experiments in GEO.
332 This meta-analysis suggests that the partitioning of the phenotypic and transcriptional stress responses
333 extends beyond the nutrient depletion stresses analyzed in this study and further suggests that the
334 phenotypic and the transcriptional response networks are composed of highly dissimilar regulatory
335 modules.
336
337

CONCLUSIONS

A popular assumption is that differentially expressed genes are good proxies for genes that are important for maintaining the survival of a microbe under stressful conditions [8-11]. Our validated genome-wide profiles for three strains of *S. pneumoniae* show in detail that genes and pathways that become important upon nutrient depletion are generally not differentially expressed. It is possible that the products of the genes that change their fitness are characterized by post-transcriptional or post-translational, rather than transcriptional, changes [40,41]. For instance, enzymes involved in protein and carbohydrate biosynthesis are heavily modified by lysine succinylation in multi-drug resistant *Mycobacterium tuberculosis* strains [42], while S-glutathionylation serves as a major regulation mechanism when *Cyanobacteria* are under oxidative stress conditions [43]. However, in general these mechanisms only affect a relatively small number of genes, and overall there seems to be a strong correlation between transcription and protein levels, especially during mid-exponential growth [44]. We thus do not believe that our findings are coincidental and related to our organism or experimental setup, also because several other studies on bacterial and fungal species have implied similar patterns in certain metabolic pathways and cellular functions, even though not all of them were validated or conducted on a genome-wide level [40,45,46]. It seems that a poor correlation between transcriptional change and functional importance is, at least for bacteria, universal. This means that transcriptomic profiling studies should be assessed carefully when they are used as a predictor of genes that matter phenotypically, e.g. in genetic engineering or drug target identification studies. Drug target identification across different domains of life has heavily relied on transcriptomic data as a surrogate for functional importance [47-53]. For instance, inhibitors of streptokinase gene expression have been proposed as novel antimicrobials for group A streptococcus [52], and gene expression datasets were used as a source for co-target identification using a random-walk model based on *M. tuberculosis* [51]. Our results provide an important argument to search for phenotypically important genes instead of differentially expressed genes in future antimicrobial discovery -- blocking differentially expressed genes may fail to cause a growth defect while phenotypically important genes directly affect an organism's fitness.

In our attempts to unify fitness and expression changes, we showed that leveraging genome-scale metabolic modeling and topological analyses links both sets of genes in a cellular metabolic network.

366 Although changes in transcription status and changes in functional importance occur on separate sets of
367 genes, our result show that these sets of genes are either in the same pathways or closely related pathways
368 that share intermediates. This pattern is consistent with the ideas of metabolic control analysis (MCA),
369 where pathway flux can be controlled by changes in either enzyme abundance or substrate concentrations
370 [39,54]. A central result of MCA is that the relative importance of enzyme or substrate changes can vary
371 along a pathway. In our example of the shikimate pathway (**Figure 5a**), the upper half of the pathway
372 (SP1371-SP1377) may be controlled by substrate abundance, while flux through the amino acid-specific
373 branches (e.g. SP1811-SP1818) may be controlled by enzyme abundance. It is important to note that all of
374 the reversible reactions in the shikimate pathway occur before the branch point (**Figure 5a**), and the
375 (reversible) enzymes above the branch point are not differentially expressed. Reversibility allows pathway
376 intermediates to control flux through feedback mechanisms, possibly lessening the importance of
377 transcriptional control in the upper branch. By deferring most of the transcriptional control until the lower
378 branches of the shikimate pathway, *S. pneumoniae* may be able to control the production of Trp separately
379 from the other aromatic amino acids while still maintaining adequate flux through the upper branch via
380 substrate-level feedback.

381 A common explanation for the lack of an expected fitness defect is redundancy in the surrounding
382 network. Since all of the fitness defects in the shikimate pathway occur before it branches into pathways
383 for individual amino acids, it is possible that redundancies exist that can overcome the loss of a
384 biosynthetic route for a single amino acid, but not for all three. Although there is no known alternative
385 route for aromatic amino acid synthesis outside of the shikimate pathway, the Trp-specific genes could be
386 redundant and thus some genes in the pathway could alleviate the absence of other genes and provide
387 functional redundancy. Identifying these “hidden” redundancies is a powerful benefit of overlaying
388 genome-scale phenotypic data onto mathematical models.

389 In addition to allowing more parsimonious gene regulatory networks, separating transcriptional
390 control from phenotypic importance may allow bacteria more flexibility to respond to new environments
391 without incurring a fitness cost. Genes that fluctuate transcriptionally are not important for sustaining
392 growth and hence have more flexibility in their expression. Phenotypically important genes seem to be
393 shielded from large, fluctuating expression changes and are possibly controlled by feedback loops, which

394 is a mechanism adept at retaining expression levels within tight boundaries [55]. Taken together, these
395 features allow a bacterium to maintain a tightly controlled, robust core of essential genes while
396 simultaneously preserving metabolic flexibility.

397 In this report, we present a transferable, systems-level approach to reconcile transcription and fitness
398 changes within a network, which serves as an important attempt to achieve a systems-level understanding
399 of how a bacterium deals with environmental perturbations. Although metabolism represents the majority
400 of genes that change in either expression or fitness during nutrient depletion (**Figure 3c**), we are striving to
401 achieve a truly holistic view by integrating additional parts of the genomic network, including energy
402 generation, cell division, transport, and formation and turnover of the cell wall and membrane. Lastly,
403 applying network topological analyses to contextualize high-throughput experiments has the potential to
404 provide value in genetic engineering, predicting drug target candidates, and re-evaluating current drug
405 targets with the goal to achieve a higher success rate in developing novel strategies to eradicate microbial
406 pathogens.

METHODS

Bacterial strains, growth and media

Experiments were performed with *S. pneumoniae* strains TIGR4 (T4; NCBI Reference Sequence: NC_003028.3) and Taiwan-19F (19F; NC_012469.1), and D39 (NC_008533). All gene numbers are according to the TIGR4 genome, except the unique genes, which are preceded by SP, SPT, and SPD for TIGR4, Taiwan-19F, and D39, respectively. A "correspondence table" that matches homologous genes in the three strains can be found in **Additional File 2**. Single gene knock-out strains were constructed by replacing the coding regions with a chloramphenicol or spectinomycin resistance cassette as described previously [2,14,56]. Except for Tn-Seq experiments, RNA-Seq experiments, and specific growth conditions, *S. pneumoniae* was cultivated statically in Todd Hewitt broth with 5% yeast extract and 5 µL/mL of Oxyrase (Oxyrase, Inc), or on sheep's blood agar plates at 37ºC in a 5% CO_2 atmosphere. When appropriate, liquid culture and blood agar plates contained 4 µg/mL of chloramphenicol (Cm) or 200 µg/mL of spectinomycin (Spec) for selecting strains or mutant libraries that contain drug markers. Tn-Seq and RNA-Seq experiments were performed in three growth media that contain gradually decreasing nutrient levels, namely, semi-defined minimal medium (SDMM) [2], chemically defined medium (CDM; **Additional File 4**) and minimal chemically defined medium (MCDM; **Additional File 4**).

Tn-Seq library construction and selection experiments

Transposon insertion mutant libraries were constructed as previously described with the transposon Magellan6, which lacks transcriptional terminators therefore allows for read-through transcription and diminishing polar effects [2,14,57]. Additionally, the mini-transposon contains stop codons in all three frames in either orientation when inserted into a coding sequence. Six independent transposon libraries were constructed in T4, 19F, and D39. Tn-Seq experiments were performed with each transposon library for each of the three strains under the three media conditions (pH 7.3 with 20mM of supplemental glucose in SDMM and MCDM and 28 mM glucose in CDM). Mutant libraries were grown to mid- to late-log phase and harvested for genomic DNA isolation.

435 **Tn-Seq sample preparation, sequencing and fitness calculation**

436 Sample preparation, Illumina sequencing, and fitness calculations were performed as previously
437 described [2,14,18,58]. For each insertion, fitness (W_i) representing the growth rate is calculated by
438 determining the change in frequency for the mutant in the population [58]. Fitness for single genes is
439 calculated by averaging W_i over all the insertions in the same gene. To determine whether fitness effects
440 significantly differ between conditions, three requirements must be fulfilled: 1.) W_i is calculated from at
441 least three data points (insertions), 2.) the difference in fitness between conditions has to be larger than
442 15% ($|W_i - W_j| > 0.15$), and 3.) the difference in fitness has to be significantly different in a one sample
443 *t*-test with Bonferroni correction for multiple testing.

444

445 **Competition and single strain growth assays**

446 1x1 competition experiments were performed by mixing a single gene knock-out strain with the
447 corresponding wild type strain in a 1:1 ratio and growing for approximately eight generations to late
448 exponential phase in a particular growth medium [2]. A sample was taken at the beginning and the end
449 of a competition experiment for CFU counts and plated on blood agar plates (for a total CFU count) and
450 on blood agar plates with selective antibiotics (for a CFU count of the knock-out strain). Fitness was
451 then calculated using the same approach as Tn-Seq by determining the ratios of the competing strains at
452 the start and end of the competition and determining the expansion of the population using CFU counts.
453 Single-strain growth assays were performed in 96-well plates by taking OD_{600} measurements on a Tecan
454 Infinite 200 PRO plate reader. Both competition and single-strain growth assays were performed no
455 fewer than three times.

456

457 **RNA-Seq sample collection**

458 The three strains were grown under each of the three growth media conditions (SDMM, CDM, and
459 MCDM) in four biological replicates. 5 mL of early mid-log phase liquid culture was harvested by
460 centrifugation at 4ºC, snap frozen, and stored at -80ºC for RNA isolation. Total RNA was isolated using
461 the RNeasy Mini kit (Qiagen).

462

463 **RNA-Seq sample preparation, sequencing and expression level calculations**

464 RNA-Seq cDNA libraries were generated following the RNAtag-Seq protocol as previously described
465 [59]. Briefly, 400ng of RNA was fragmented, depleted of genomic DNA using TURBO DNA-free kit
466 (Ambion), 5'-dephosphorylated, and subsequently ligated to barcoded RNA adapters at the 3'-terminus.
467 Barcoded RNA samples were pooled and purified with RiboZero (Illumina). The ribosomal
468 RNA-depleted samples were converted to Illumina cDNA sequencing libraries in three key steps: 1.)
469 First strand cDNA synthesis with AffinityScript Multiple Temperature cDNA Synthesis kit (Agilent) and
470 RNA degradation, 2.) ligation to a 3'-linker, and 3.) PCR amplification using primers that target the
471 3'-linker and a constant region of the RNA barcodes and contain the Illumina flow cell sequences. The
472 cDNA libraries were sequenced on an Illumina NextSeq500 platform (single read, 50 base pair).

473 Raw reads were demultiplexed, trimmed to 40 base pairs, and quality filtered using custom R
474 scripts and the ShortRead package. Reads were mapped to the corresponding *S. pneumoniae* genome
475 using Bowtie [60] with settings "-n 2 -l 60 -m 1 -B 1". Reads were aggregated to genes using the
476 GenomicRanges R package and differential expression was calculated using DESeq2 [61].

477

478 **qPCR expression analysis**

479 The three wildtype strains were grown in SDMM, CDM, and MCDM to early mid-log phase. Sample
480 collection and total RNA isolation were performed following the same procedure as RNA-Seq. 4 ug of
481 RNA from each sample was treated with the TURBO DNA-free kit, after which 400 ng of cleaned-up
482 RNA was subjected to first strand cDNA synthesis using iScript reverse transcription Supermix
483 (BioRad). Quantitative PCR was performed using a BioRad MyiQ; each sample was measured in two
484 biological replicates and three technical replicates. No-reverse transcriptase and no-template controls
485 were included for each sample. Expression levels from all samples were normalized against the 50S
486 ribosomal gene SP2204.

487

488 **Statistical analysis**

489 Statistical analyses were performed in R (http://www.r-project.org). Gene distributions were fit to either
490 Poisson (gene distance distributions) or Gamma (GEO plasticity) distributions using the fitdistr function

491 in the MASS toolbox. Expected values of the distributions were compared by a *t*-test.

492

493 **DECLARATIONS**

494 **Ethics approval and consent to participate**. Not applicable.

495 **Consent for publication**. Not applicable.

496 **Availability of data and materials**. The datasets generated during the current study are available as
497 Additional Files and in the Sequence Read Archive (SRP082544).

498 **Competing interests**. The authors declare that they have no competing interests.

499 **Funding**. This work was supported by the NIH R01 AI110724 and U01 AI124302.

500 **Authors' contributions**. PAJ led the computational experiments. ZZ led the wet-lab experiments. PAJ
501 and ZZ performed computational and wet-lab experiments. All authors analyzed data, interpreted results,
502 and wrote and approved the final manuscript.

503 **Acknowledgements**. DNA sequencing was performed at the Boston College Sequencing Core.

504

505 **ADDITIONAL FILES**

506 **Additional File 1:** *S. pneumoniae* phylogenetic tree.

507 **Additional File 2:** Gene correspondence table.

508 **Additional File 3:** Breakdown of *S. pneuomniae* genes by strain and category.

509 **Additional File 4:** Media composition for SDMM, CDM, and MCDM.

510 **Additional File 5:** Growth curves for T4, 19F, and D39 in SDMM, CDM, and MCDM.

511 **Additional File 6:** Tn-Seq and RNA-seq data

512 **Additional File 7:** Tn-Seq validation

513 **Additional File 8:** RNA-seq validation

514 **Additional File 9:** Supplementary Methods: Model assembly and curation; minor metabolite listing;
515 GEO datasets and analysis pipeline.

516 **Additional File 10:** iSP16 model in SBML format.

517 **Additional File 11:** Essential genes for T4, 19F, and D39.

518

519 **REFERENCES**

520 1. van Opijnen T, Dedrick S, Bento J. Strain-specific antibiotic sensitivity in *S. pneumoniae*. PLoS
521 Pathog. 2016. In Press.

522 2. van Opijnen T, Camilli A. A fine scale phenotype-genotype virulence map of a bacterial pathogen.
523 Genome Research. 2012;22:2541–51.

524 3. Drlica K, Malik M, Kerns RJ, Zhao X. Quinolone-Mediated Bacterial Death. Antimicrob. Agent
525 Chemother. 2008;52:385–92.

526 4. Tomasz A. The Mechanism of The Irreversible Antimicrobial Effects of Penicillins: How the
527 Beta-Lactam Antibiotics Kill and Lyse Bacteria. Annu Rev Microbiol. 1979;:1–25.

528 5. Vakulenko SB, Mobashery S. Versatility of Aminoglycosides and Prospects for Their Future. Clin
529 Microbiol Rev. 2003;16:430–50.

530 6. Floss HG, Yu T-W. RifamycinMode of Action, Resistance, and Biosynthesis. Chem. Rev.
531 2005;105:621–32.

532 7. Rajagopal M, Martin MJ, Santiago M, Lee W, Kos VN, Meredith T, et al. Multidrug Intrinsic
533 Resistance Factors in Staphylococcus aureusIdentified by Profiling Fitness within High-Diversity
534 Transposon Libraries. mBio. 2016;7:e00950–16–11.

535 8. Chatterjee A, Saranath D, Bhatter P, Mistry N. Global Transcriptional Profiling of Longitudinal
536 Clinical Isolates of Mycobacterium tuberculosis Exhibiting Rapid Accumulation of Drug Resistance.
537 Dheda K, editor. PLoS ONE. 2013;8:e54717–8.

538 9. Nielsen PK, Andersen AZ, Mols M, van der Veen S, Abee T, Kallipolitis BH. Genome-wide
539 transcriptional profiling of the cell envelope stress response and the role of LisRK and CesRK in
540 Listeria monocytogenes. Microbiology. 2012;158:963–74.

541 10. Bao H, Kommadath A, Liang G, Sun X, Arantes AS, Tuggle CK, et al. Genome-wide whole blood
542 microRNAome and transcriptome analyses reveal miRNA-mRNA regulated host response to
543 foodborne pathogen Salmonella infection in swine. Sci Rep. 2015;:1–12.

544 11. Butcher J, Stintzi A. The Transcriptional Landscape of Campylobacter jejuni under Iron Replete
545 and Iron Limited Growth Conditions. Zhang Q, editor. PLoS ONE. 2013;8:e79475–16.

546 12. Guimaraes JC, Rocha M, Arkin AP. Transcript level and sequence determinants of protein
547 abundance and noise in Escherichia coli. Nucleic Acids Research. 2014;42:4791–9.

548 13. Feder ME, Walser JC. The biological limitations of transcriptomics in elucidating stress and
549 stress responses. J Evolution Biol. 2005;18:901–10.

550 14. van Opijnen T, Bodi KL, Camilli A. Tn-seq: high-throughput parallel sequencing for fitness and
551 genetic interaction studies in microorganisms. Nat Meth; 2009;:1–9.

552 15. Langridge GC, Phan MD, Turner DJ, Perkins TT, Parts L, Haase J, et al. Simultaneous assay of
553 every Salmonella Typhi gene using one million transposon mutants. Genome Research.
554 2009;19:2308–16.

555 16. Gawronski JD, Wong SM, Giannoukos G, Ward DV, Akerley BJ. Tracking insertion mutants
556 within libraries by deep sequencing and a genome-wide screen for Haemophilus genes required in
557 the lung. PNAS. 2009:1–6.

558 17. Goodman AL, McNulty NP, Zhao Y, Leip D, Mitra RD, Lozupone CA, et al. Identifying Genetic
559 Determinants Needed to Establish a Human Gut Symbiont in Its Habitat. Cell Host & Microbe.
560 2009;6:279–89.

561 18. van Opijnen T, Camilli A. Transposon insertion sequencing: a new tool for systems-level
562 analysis of microorganisms. Nat Rev Microbiol. 2013;11:435–42.

563 19. Tuomanen EI, Mitchell TJ, Morrison BG. The Pneumococcus. Washington: ASM Press.

564 20. CDC. Antibiotic Resistance Threats in the United States. 2013;1–114.

565 21. WHO. Pneumococcal conjugate vaccine for childhood immunization--WHO position paper.
566 Relevé épidémiologique hebdomadaire Section dhygiène du Secrétariat de la Société des Nations
567 Weekly epidemiological record Health Section of the Secretariat of the League of Nations.
568 2007;93–104.

569 22. Henriques-Normark B, Tuomanen EI. The Pneumococcus: Epidemiology, Microbiology, and
570 Pathogenesis. Cold Spring Harbor Perspectives in Medicine. 2013;3:a010215–5.

571 23. Medini D, Serruto D, Parkhill J, Relman DA, Donati C, Moxon R, et al. Microbiology in the
572 post-genomic era. Nat Rev Microbiol. 2008;1–12.

573 24. Medini D, Donati C, Tettelin H, Masignani V, Rappuoli R. The microbial pan-genome. Curr Opin
574 Genet Dev. 2005;15:589–94.

575 25. Tenaillon O, Skurnik D, Picard B, Denamur E. The population genetics of commensal
576 Escherichia coli. Nat Rev Microbiol. 2010;8:207–17.

577 26. Boone C, Bussey H, Andrews BJ. Exploring genetic interactions and networks with yeast. Nat.
578 Rev. Genet. 2007;8:437–49.

579 27. Dixon SJ, Costanzo M, Baryshnikova A, Andrews B, Boone C. Systematic mapping of genetic
580 interaction networks. Annu. Rev. Genet. 2009;43:601–25.

581 28. Aaberge IS, Eng J, Lermark G, Lovik M. Virulence of Streptococcus pneumoniae in mice: a
582 standardized method for preparation and frozen storage of the experimental bacterial inoculum.
583 Microbial Pathogenesis. 1995;1–12.

584 29. Tettelin H, Ciammola A, Rigamonti D, Leavitt BR, Goffredo D, Conti L, et al. Complete Genome
585 Sequence of a Virulent Isolate of Streptococcus pneumoniae. Science. 2001;293:493–8.

586 30. McGee L, McDougal L, Zhou J, Spratt BG, Tenover FC, George R, et al. Nomenclature of major
587 antimicrobial-resistant clones of Streptococcus pneumoniae defined by the pneumococcal
588 molecular epidemiology network. Journal of Clinical Microbiology. 2001;39:2565–71.

589 31. Shi Z-Y, Enright MC, Wilkinson P, Griffiths D, Spratt BG. Identification of Three Major Clones of
590 Multiply Antibiotic- Resistant. Journal of Clinical Microbiology. 1998;:1–6.

591 32. Lanie JA, Ng WL, Kazmierczak KM, Andrzejewski TM, Davidsen TM, Wayne KJ, et al. Genome
592 Sequence of Avery's Virulent Serotype 2 Strain D39 of Streptococcus pneumoniae and Comparison
593 with That of Unencapsulated Laboratory Strain R6. J. Bacteriol. 2006;189:38–51.

594 33. Härtel T, Eylert E, Schulz C, Petruschka L, Gierok P, Grubmüller S, et al. Characterization of
595 central carbon metabolism of Streptococcus pneumoniae by isotopologue profiling. J. Biol. Chem.
596 2012;287:4260–74.

34. Haas BJ, Chin M, Nusbaum C, Birren BW, Livny J. How deep is deep enough for RNA-Seq profiling of bacterial transcriptomes? BMC Genomics. 2012;1–11.

35. Department of Energy Systems Biology Knowledgebase (KBase), http://kbase.us.

36. Satish Kumar V, Dasika MS, Maranas CD. Optimization based automated curation of metabolic reconstructions. BMC Bioinformatics. 2007;8:212–6.

37. Kanehisa M, Goto S, Sato Y, Furumichi M, Tanabe M. KEGG for integration and interpretation of large-scale molecular data sets. Nucleic Acids Research. 2011;40:D109–14.

38. Karp P, Billington R, Holland T, Kothari A, Krummenacker M, Weaver D, et al. Computational Metabolomics Operations at BioCyc.org. Metabolites. 2015;5:291–310.

39. Fell D. Understanding The Control of Metabolism. London: Portland Press; 1997.

40. Giaever G, Chu AM, Ni L, Connelly C, Riles L, Veronneau S, et al. Functional profiling of the Saccharomyces cerevisiae genome. Nature. 2002;1–5.

41. Grangeasse C, StÃ¼lke JR, Mijakovic I. Regulatory potential of post-translational modifications in bacteria. Front. Microbiol. 2015;6:1–2.

42. Xie L, Liu W, Li Q, Chen S, Xu M, Huang Q, et al. First Succinyl-Proteome Profiling of Extensively Drug-Resistant Mycobacterium tuberculosisRevealed Involvement of Succinylation in Cellular Physiology. J. Proteome Res. 2015;14:107–19.

43. Chardonnet S, Sakr S, Cassier-Chauvat C, Le Maréchal P, Chauvat F, Lemaire SD, et al. First Proteomic Study of S-Glutathionylation in Cyanobacteria. J. Proteome Res. 2015;14:59–71.

44. Taylor RC, Webb Robertson B-JM, Markillie LM, Serres MH, Linggi BE, Aldrich JT, et al. Changes in translational efficiency is a dominant regulatory mechanism in the environmental response of bacteria. Integr. Biol. 2013;5:1393–14.

45. Price MN, Deutschbauer AM, Skerker JM, Wetmore KM, Ruths T, Mar JS, et al. Indirect and suboptimal control of gene expression is widespread in bacteria. Mol Syst Biol. Nature Publishing Group; 2013;9:1–18.

622 46. Turner KH, Everett J, Trivedi U, Rumbaugh KP, Whiteley M. Requirements for Pseudomonas
623 aeruginosa Acute Burn and Chronic Surgical Wound Infection. Garsin DA, editor. PLoS Genet.
624 2014;10:e1004518–12.

625 47. Patil SD, Sharma R, Srivastava S, Navani NK, Pathania R. Downregulation of yidC in Escherichia
626 coli by Antisense RNA Expression Results in Sensitization to Antibacterial Essential Oils Eugenol
627 and Carvacrol. van Veen HW, editor. PLoS ONE. 2013;8:e57370–9.

628 48. Fadhal E, Mwambene E, Gamiedien J. Modelling human protein interaction networks as metric
629 spaces has potential in disease research and drug target discovery. BMC Syst Biol. 2014;:1–12.

630 49. Mizuarai S, Yamanaka K, Itadani H, Arai T, Nishibata T, Hirai H, et al. Discovery of gene
631 expression-based pharmacodynamic biomarker for a p53 context-specific anti-tumor drug Wee1
632 inhibitor. Mol Cancer. 2009;8:34–12.

633 50. Liu M, Healy MD, Dougherty BA, Esposito KM, Maurice TC, Mazzucco CE, et al. Conserved
634 Fungal Genes as Potential Targets for Broad-Spectrum Antifungal Drug Discovery. Eukaryotic Cell.
635 2006;5:638–49.

636 51. Chen L-C, Yeh H-Y, Yeh C-Y, Arias CR, Soo V-W. Identifying co-targets to fight drug resistance
637 based on a random walk model. BMC Syst Biol. 2012;:1–14.

638 52. Sun H, Xu Y, Sitkiewicz I, Ma Y, Wang X, Yestrepsky BD, et al. Inhibitor of streptokinase gene
639 expression improves survival after group A streptococcus infection in mice. PNAS. 2012;:1–6.

640 53. Mukhopadhyay S, Nair S, Ghosh S. Pathogenesis in tuberculosis: transcriptomic approaches to
641 unraveling virulence mechanisms and finding new drug targets. FEMS Microbiol Rev.
642 2012;36:463–85.

643 54. Heinrich R, Schuster D. The Regulation of Cellular Systems. Boston: Springer; 1996.

644 55. Shah NA, Sarkar CA. Robust Network Topologies for Generating Switch-Like Cellular
645 Responses. PLoS Comp Biol. 2011;1–12.

646 56. Iyer R, Baliga NS, Camilli A. Catabolite Control Protein A (CcpA) Contributes to Virulence and
647 Regulation of Sugar Metabolism in Streptococcus pneumoniae. J. Bacteriol. 2005;187:8340–9.

57. van Opijnen T, Lazinski DW, Camilli A. Genome-Wide Fitness and Genetic Interactions Determined by Tn-seq, a High-Throughput Massively Parallel Sequencing Method for Microorganisms. Curr Protoc Mol Biol. 2015;36:1E.3.1–1E.3.24.

58. van Opijnen T, Boerlijst MC, Berkhout B. Effects of Random Mutations in the Human Immunodeficiency Virus Type 1 Transcriptional Promoter on Viral Fitness in Different Host Cell Environments. J.Virol. 2006;80:6678–85.

59. Shishkin AA, Giannoukos G, Kucukural A, Ciulla D, Busby M, Surka C, et al. Simultaneous generation of many RNA-seq libraries in a single reaction. Nat Meth. 2015;12:323–5.

60. Langmead, B., Trapnell, C., Pop, M., & Salzberg, S. L. (2009). Ultrafast and memory-efficient alignment of short DNA sequences to the human genome. *Genome Biology*, *10*(3), R25. http://doi.org/10.1186/gb-2009-10-3-r25

61. Love MI, Huber W, Anders S. Moderated estimation of fold change and dispersion for RNA-seq data with DESeq2. Genome Biology. 2014;15:31–21.

663

664 **Table 1** Summary of the three *S. pneumoniae* strains in this study

Strains	TIGR4	Taiwan-19F	D39
RefSeq	NC_003028	NC_012469	NC_008533
Genome size (bp)	2,160,842	2,112,148	2,046,115
Number of genes	2287	2119	2165
Origin	Isolated from the blood of a 30-year-old male patient in Kongsvinger, Norway	A patient with invasive pneumococcal disease in Taiwan	Clinical isolate, 1916
Reference	Aaberge *et al.* (1995) Tettelin *et al.* (2001)	Shi *et al.* (1995) McGee *et al.* (2001)	Lanie *et al.* (2006)
Doubling time (min)			
SDMM	51 ± 5	74 ± 2	57 ± 4
CDM	80 ± 7	110 ± 10	74 ± 4
MMCDM	108 ± 9	118 ± 13	100 ± 8

665

666 **Table 2**. Comparison of nutrient availability in SDMM, CDM and MCDM.

Components	SDMM	CDM	MCDM
Casein Hydrolysate	X		
Yeast Extract	X		
L-Ala		X	
L-Arg		X	X
L-Asn	X	X	
L-Asp		X	
L-Cys	X	X	X
L-Gln	X	X	X
L-Glu		X	
Gly		X	X
L-His		X	X
L-Ile		X	X
L-Leu		X	X
L-Lys		X	
L-Met		X	X
L-Phe		X	
L-Pro		X	X
L-Ser		X	X
L-Thr		X	X
L-Trp	X	X	
L-Tyr		X	
L-Val		X	X
Adenine	X	X	X
Uracil	X	X	X*
Ca-Pantothenate	X	X	X
Nicotinic Acid	X	X	X
Pyridoxine.HCL	X	X	
Thiamine.HCL	X	X	
Riboflavine	X	X	
Biotin	X	X	

K2HPO4	X	X	X
NaOAc	X	X	X
NaHCO3	X	X	X
MgCl2.6H2O	X	X	X
CaCl2	X	X	X
CuSO4.5H2O	X	X	X
ZnSO4.7H2O	X	X	X
MnSO4.4H2O	X	X	X
D-Glucose	X	X	X

X: present in a medium.

* In MCDM uracil was supplied at half the concentration compared to SDMM (**Additional File 4**).

671 **FIGURE LEGENDS**

672

673 Figure 1: High-resolution profiles of phenotype and gene expression during stress incurred by nutrient
674 depletion. **A**. Fitness values from Tn-Seq. **B**. Transcript abundance from RNA-Seq. Both
675 high-throughput methods were performed on three *S. pneumoniae* strains (19F, T4, and D39) and in
676 three media conditions (SDMM, CDM, and MCDM). **C**. By plotting Tn-Seq and RNA-Seq data on the
677 same graph it becomes clear that genes with fitness defects ($W < 0.85$) are highly expressed.

678

679 Figure 2: Tn-Seq and RNA-Seq data correlate strongly with validation experiments. **A**. A strong
680 correlation between Tn-Seq fitness and fitness calculated from individual mutant growth curves or 1x1
681 competitions ($W_{validation}$; n = 122; shown are mean ± SEM; linear fit yields $R^2 > 0.82$) emphasizes that
682 the strain-dependent sensitivity profiles are composed of high-confidence Tn-Seq data. **B.**
683 Representative growth curves for comparisons between wild type (WT) and mutant ΔSP1376 in three
684 different conditions, showing the dependence of the mutant on the presence of aromatic amino acids in
685 the environment. **C**. Fold change in transcript abundance measured by qPCR and RNA-Seq. Vertical
686 bars indicate SEM for both experiments. No qPCR and RNA-Seq pairs differed significantly ($p < 0.0042$,
687 *t*-test with Bonferroni correction) indicating RNA-Seq data are composed of high-confidence data as
688 well.

689

690 Figure 3: Changes in gene fitness and expression occur across all strains, media, and cellular subsystems.
691 **A**. Δ*fitness (ΔW)* depicts how genes change their fitness as a strain transitions from rich media (SDMM)
692 to defined (CDM) or minimal (MCDM) media. **B**. Shown are how genes change their expression as a
693 strain transitions from rich media (SDMM) to defined (CDM) or minimal (MCDM) media. Expression
694 is $\log_2$ fold change in transcript abundance from RNA-Seq. In both figures statistically significant
695 changes are colored and both assays were performed on three *S. pneumoniae* strains (T4, 19F, and D39)
696 and two media transitions (SDMM→CDM, SDMM→MCDM). **C**. Percentage of genes in each category
697 with significant changes in fitness (red) and expression (green). For total number of genes in each
698 category (by strain), see **Additional File 3**.

699

700 Figure 4: Genes with significant changes in expression (green), fitness (red), or both (blue) are
701 distributed throughout the iSP16 metabolic model. Lines indicate reactions connecting metabolites
702 (circles). Minor and currency metabolites are not shown (see **Additional File 9**). Reactions are colored
703 based on gene associations in the iSP16 model.

704

705 Figure 5: Fitness and expression changes do not occur on the same gene but appear to be related. **A**.
706 Changes in gene expression and fitness are separated in the tryptophan biosynthesis branch of the
707 shikimate pathway. Single and double-headed arrows indicate reversibility or non-reversibility of
708 individual chemical reactions, respectively, while arrows spanning two genes indicate enzymatic
709 subunits catalyzing the same reaction. The dashed blue line (between SP1374 and SP1816) indicates the
710 branch point into tryptophan biosynthesis. PEP=phosphoenol-pyruvate, E4P=*D*-erythrose-4-phosphate,
711 Trp=*L*-tryptophan. **B**. Changes in gene expression (RNA-Seq: Δ*expression*) vs. changes in fitness
712 (Tn-Seq: Δ*fitness (ΔW)*) are not correlated. For each data point (gene) Δ*fitness (ΔW)* and Δ*expression* are
713 plotted depicting how a gene's fitness and expression change as a strain transitions from rich media
714 (SDMM) to defined (CDM) or minimal (MCDM) media. **C**. Genes with significant Δ*expression* or
715 Δ*fitness (ΔW)* (black) migrate off the horizontal and vertical axes when paired with the nearest neighbor
716 that changes in fitness or expression (red) (NB. If multiple genes appear at the same distance from the
717 gene with a fitness change, the expression changes are averaged.). **D**. The number of genes in each
718 quadrant of the Δ*expression*/Δ*fitness* plot shifts before (black) and after (red) nearest-neighbor pairing,
719 showing that fitness and expression changes are somehow linked.

720

721 Figure 6: Metabolic models can quantify distances between reactions and genes. **A**. Shown is how
722 distances are calculated. For instance, the distance between the subunits *pgmA* and *pgmB* in glycolysis is
723 zero, while either enzyme has a distance one to *eno* and a distance two to *pyk*. **B**. The area off axes is the
724 product of Δ*expression* and Δ*fitness (ΔW)* and is maximized when both the fitness and expression
725 changes are large. The area off axes is near zero when either the fitness or expression change is small. **C**.
726 Extent of off-axis migration after nearest-neighbor averaging decays with distance between the gene and

its nearest neighbor, indicating that changes are closely located within the network and that the largest changes in fitness are close to the largest expression changes. **D**. Distribution of network distances varies between genes with fitness and expression changes. Distances between all genes (*any*), genes with significant changes in expression (*Δexpression*) or fitness (*Δfitness*). Unconnected genes (distance = ∞) are not shown. The short distances between two genes with expression changes or two genes with fitness changes indicates small subnetworks of either fitness or expression changes. **E**. Essential genes and genes with fitness or expression changes are not evenly distributed. On average, essential genes (*essential*) are closest to genes with fitness changes (*Δfitness*) and farthest from genes with expression changes (*Δexpression*).

Figure 7: Meta-analysis shows that essential and phenotypically important genes are shielded from large changes in expression. **A**. Quantifying gene expression plasticity using meta-analysis of GEO expression studies. Plasticity is the normalized variance in gene expression across all *S. pneumoniae* data in GEO (see **Additional File 9**). **B**. Gene expression plasticity is significantly lower for essential genes ($p < 10^{-14}$) and conditionally essential genes (genes with a significant fitness change) ($p < 10^{-34}$, both comparisons *t*-test on means of fitted Gamma distributions). Both the essential and conditionally essential genes appear to be shielded from transcriptional changes not only in our RNA-Seq data, but across all the expression datasets in GEO. **C**. Gene expression plasticity decreases with increasing magnitude of the fitness change (relative to SDMM). Thus the amount of shielding is proportional to a gene's phenotypic importance, and genes with the largest fitness changes show the smallest variation in expression across the experiments in GEO.

Figure 1

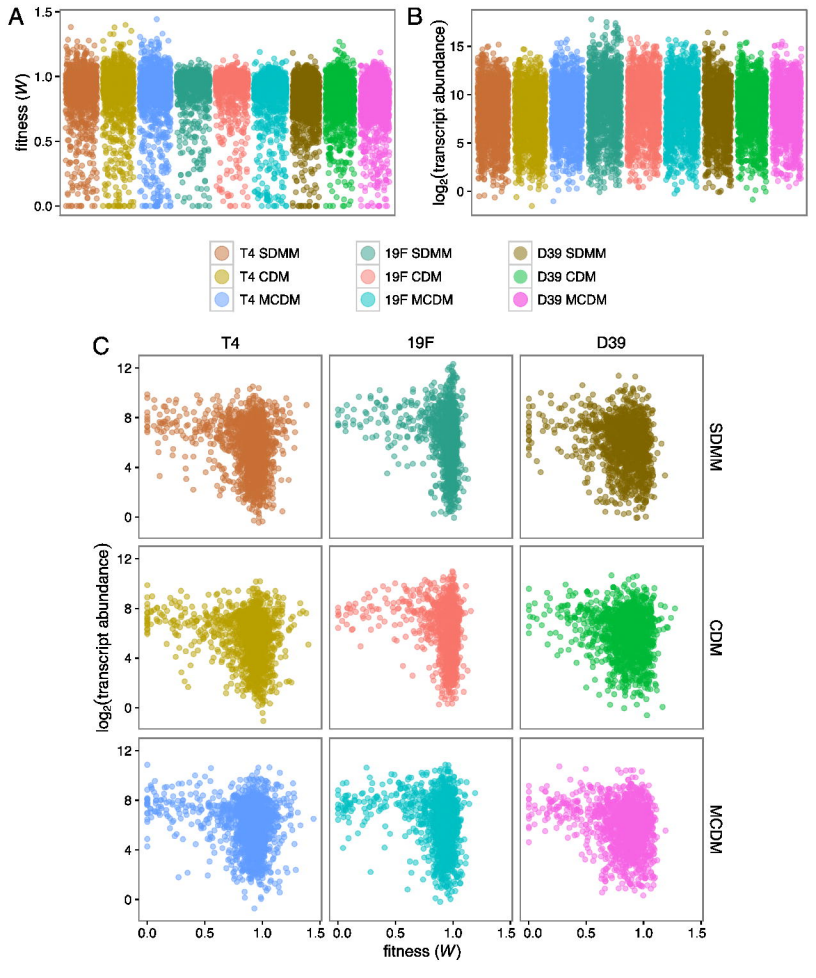
A
fitness (W)
1.5
1.0
0.5
0.0
B
log2(transcript abundance)
15
10
5
0
T4 SDMM
T4 CDM
T4 MCDM
19F SDMM
19F CDM
19F MCDM
D39 SDMM
D39 CDM
D39 MCDM
C
T4
19F
D39
SDMM
CDM
MCDM
log2(transcript abundance)
12
8
4
0
0.0
0.5
1.0
1.5
fitness (W)

Figure 2

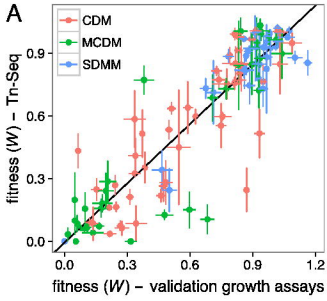
A
CDM
MCDM
SDMM
fitness (W) – Tn-Seq
fitness (W) – validation growth assays
0.0
0.3
0.6
0.9
1.2

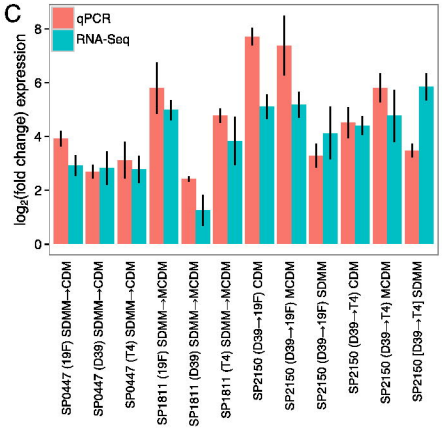
C
qPCR
RNA-Seq
log2(fold change) expression
SP0447 (19F) SDMM→CDM
SP0447 (D39) SDMM→CDM
SP0447 (T4) SDMM→CDM
SP1811 (19F) SDMM→MCDM
SP1811 (D39) SDMM→MCDM
SP1811 (T4) SDMM→MCDM
SP2150 (D39→19F) CDM
SP2150 (D39→19F) MCDM
SP2150 (D39→19F) SDMM
SP2150 (D39→T4) CDM
SP2150 (D39→T4) MCDM
SP2150 [D39→T4] SDMM

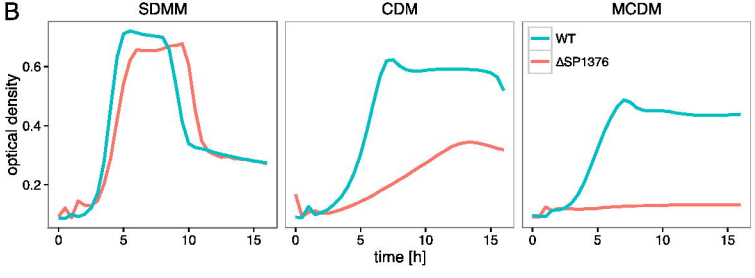
B
SDMM
CDM
MCDM
WT
ΔSP1376
optical density
time [h]

Figure 3

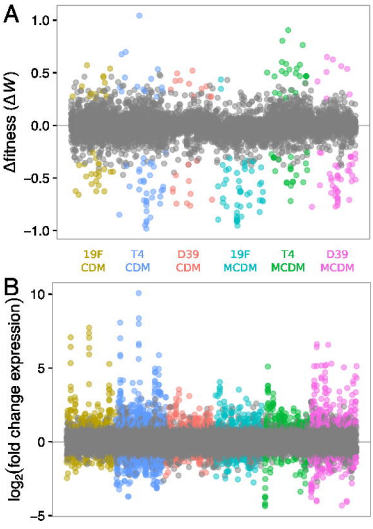
A
Δfitness (Δ W)
1.0
0.5
0.0
−0.5
−1.0
19F CDM
T4 CDM
D39 CDM
19F MCDM
T4 MCDM
D39 MCDM
B
log2(fold change expression)
10
5
0
−5

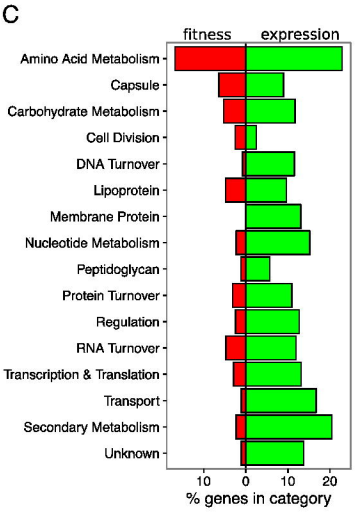
C
fitness
expression
Amino Acid Metabolism
Capsule
Carbohydrate Metabolism
Cell Division
DNA Turnover
Lipoprotein
Membrane Protein
Nucleotide Metabolism
Peptidoglycan
Protein Turnover
Regulation
RNA Turnover
Transcription & Translation
Transport
Secondary Metabolism
Unknown
10
0
10
20
% genes in category

Figure 4

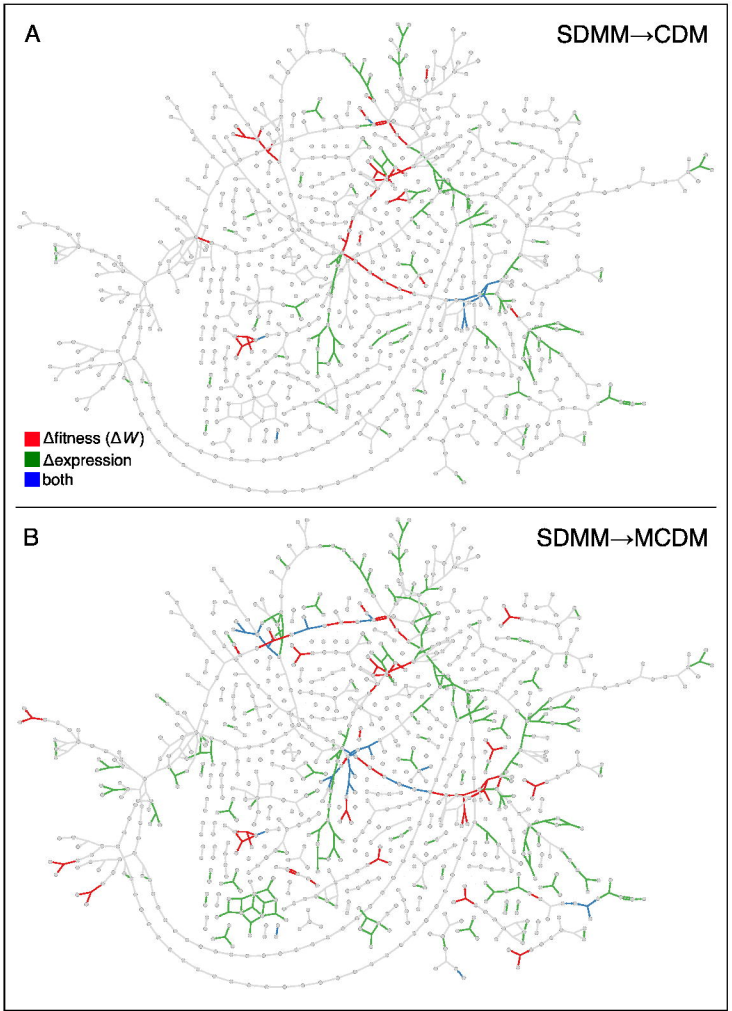

Figure 5

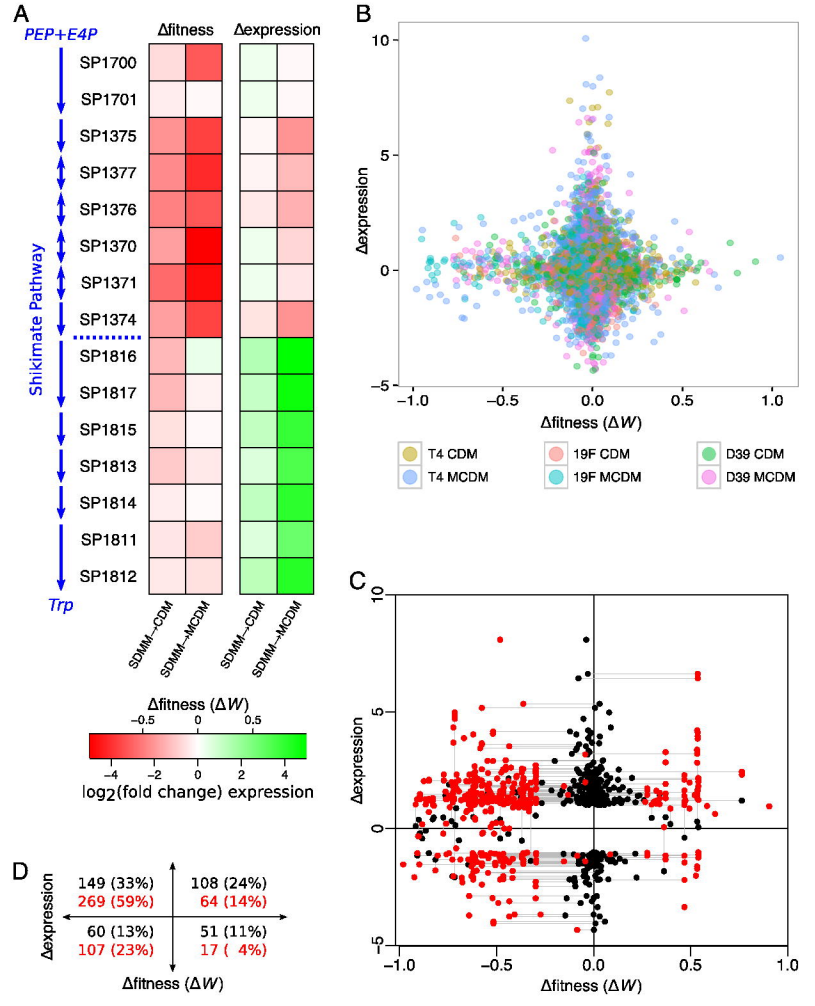
A
PEP+E4P
Δfitness
Δexpression
SP1700
SP1701
SP1375
SP1377
SP1376
SP1370
SP1371
SP1374
SP1816
SP1817
SP1815
SP1813
SP1814
SP1811
SP1812
Shikimate Pathway
Trp
SDMM→CDM
SDMM→MCDM
SDMM→CDM
SDMM→MCDM
Δfitness (ΔW)
−0.5
0
0.5
−4
−2
0
2
4
log2(fold change) expression
B
Δexpression
Δfitness (ΔW)
T4 CDM
T4 MCDM
19F CDM
19F MCDM
D39 CDM
D39 MCDM
C
Δexpression
Δfitness (ΔW)
D
Δexpression
149 (33%)
269 (59%)
108 (24%)
64 (14%)
60 (13%)
107 (23%)
51 (11%)
17 (4%)
Δfitness (ΔW)

Figure 6

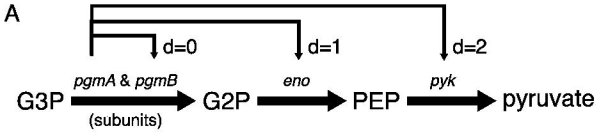
A
d=0
d=1
d=2
pgmA & pgmB
(subunits)
eno
pyk
G3P
G2P
PEP
pyruvate

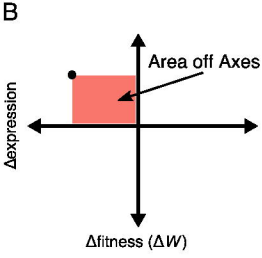
B
Area off Axes
Δexpression
Δfitness (ΔW)

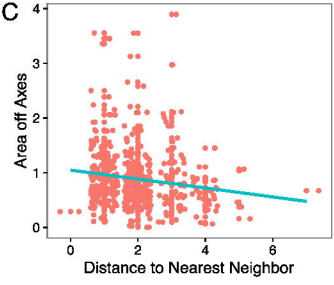
C
Area off Axes
Distance to Nearest Neighbor

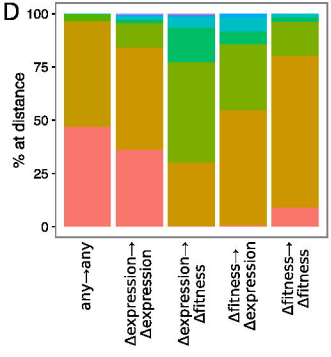
D
% at distance
any→any
Δexpression→ Δexpression
Δexpression→ Δfitness
Δfitness→ Δexpression
Δfitness→ Δfitness

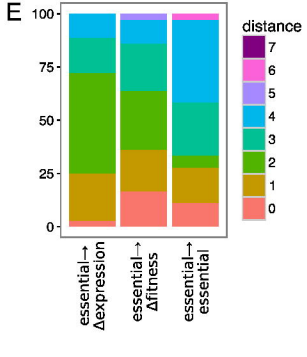
E
distance
essential→ Δexpression
essential→ Δfitness
essential→ essential

Figure 7

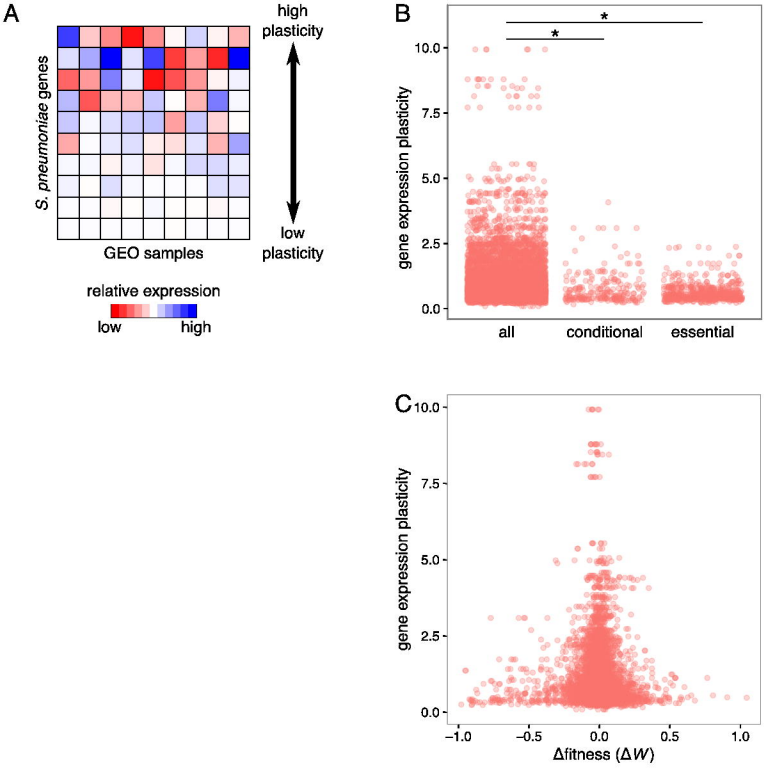
A
high plasticity
low plasticity
S. pneumoniae genes
GEO samples
relative expression
low
high
B
gene expression plasticity
10.0
7.5
5.0
2.5
0.0
*
*
all
conditional
essential
C
gene expression plasticity
10.0
7.5
5.0
2.5
0.0
−1.0
−0.5
0.0
0.5
1.0
Δfitness (Δ W)